Inorganic Chemistry

ARTICLE

pubs.acs.org/IC

On the Mechanism of the Copper-Mediated C−S Bond Formation in the Intramolecular Disproportionation of Imine Disulfides

Tibor András Rokob, Lubomír Rulíšek,* Jiří Šrogl, Ágnes Révész, Emilie L. Zins,† and Detlef Schröder*

Institute of Organic Chemistry and Biochemistry, Academy of Sciences of the Czech Republic, Flemingovo nám. 2, 16610 Prague 6, Czech Republic

Supporting Information

ABSTRACT: The mechanism of the copper-mediated disproportionation of aromatic imine disulfides to benzothiazoles in the gas phase is investigated by experimental and theoretical methods. Application of infrared multiphoton dissociation and hydrogen/deuterium exchange experiments combined with density functional theory (DFT) calculations of the relevant molecular structures and the associated infrared spectra allows the identification of the observed ionic intermediates. The theoretical investigation of the possible reaction pathways supported by collision-induced dissociation experiments provides a consistent mechanistic picture of the reaction catalyzed by a single copper(I) ion. Activation of the substrate proceeds via homolytic sulfur−sulfur bond cleavage, yielding metal complexes in the formal +3 oxidation state; carbon−sulfur coupling and hydrogen-atom transfer complete the transformation to the products. Exploratory studies demonstrate that in the gas phase, the disproportionation of the imine disulfide can also be mediated by other metal ions via different either homo- or heterolytic mechanisms without involving high-valent intermediates.

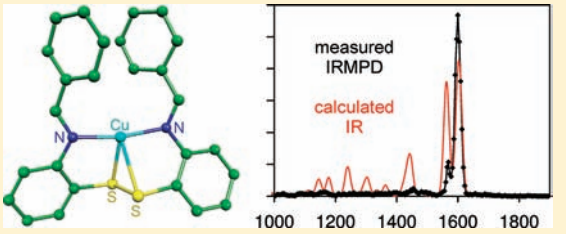

INTRODUCTION

Metal-catalyzed carbon−heteroatom coupling reactions are of great interest in contemporary chemistry and synthetic strategy.[1] Typically, these procedures involve a substrate, like an aryl halide Ar−X (X = Cl, Br, I) and a heterocomponent RY−H (Y = O, S, NH, etc.), which upon interaction with a catalyst yield the corresponding coupling product (reaction 1); often a base is added to remove the HX formed.

$$\mathrm{Ar{-}X} + \mathrm{RY{-}H} \xrightarrow{\text{catalyst}} \mathrm{Ar{-}YR} + \mathrm{H{-}X} \qquad (1)$$

Recently, some of us reported a related intramolecular reaction, in which a Cu(I) catalyst efficiently converts aromatic imine disulfides into benzothiazoles.[2] Under inert gas, a 1:1 mixture of the corresponding benzothiazole and its dihydroderivative is obtained, of which the latter is easily oxidized in the presence of air, leading to a nearly quantitative yield of the heteroaromatic product (Scheme 1). The reaction was shown to provide a convenient route to synthesize functionalized benzothiazoles,[3] which are compounds of significant pharmaceutical interest.[4]

By means of direct monitoring of the reactive solution using electrospray ionization (ESI)[5,6] mass spectrometry, it was demonstrated that a single copper atom is sufficient for providing a plausible mechanistic rationale.[2,7,8] However, the detailed reaction mechanism has been unknown.

For several transition metals, such as cobalt,[9] nickel,[10] ruthenium,[11] palladium,[12,13] and platinum,[12] oxidative addition into the S−S bond of disulfides is well-established. Accordingly, the title reaction could proceed via an analogous insertion of Cu(I) to form a transient Cu(III) dithiolato intermediate. In general, the availability of the copper(III) oxidation state is a key factor in numerous processes. Besides its proposed participation in biological dioxygen activation,[14] the involvement of Cu(III) species has been shown in several synthetically important carbon−carbon[15] and carbon−heteroatom[16] bond formation reactions, the aziridination of olefins via copper(III)-bound nitrenes,[17] the functionalization of aromatic C−H bonds,[18] or the copper-catalyzed cycloaddition of azides and terminal acetylenes.[19] While thiolates are usually prone to oxidation even by Cu(II), via application of appropriate electron-donating ligands,[20] stable bis(μ-thiolato)dicopper(II)[21] is accessible, and even diamido-dithiolato-copper(III) complexes[22] have been successfully prepared by electrochemical oxidation. Recently, reaction of copper(I) ions with a pseudopeptidic disulfide was even shown to directly produce copper(III) dithiolate,[23] although in this case the oxidation of the metal is stepwise with detectable copper(II) intermediates. We furthermore note that a possible involvement of homolytic S−S bond cleavage concomitant with a copper-coordinated diradical [formally a copper(III) species] was also proposed for C−S bond formation reactions between phenolates and disulfide-bridged dicopper(I) complexes.[24]

An alternative mechanistic scenario for the title reaction could be the involvement of a multiply centered transition structure (MCTS),[25] which enables simultaneous breaking of the S−S

Received: March 4, 2011
Published: September 20, 2011

Scheme 1. Copper-Mediated Formation of Benzothiazole from an Imine Disulfide Precursor

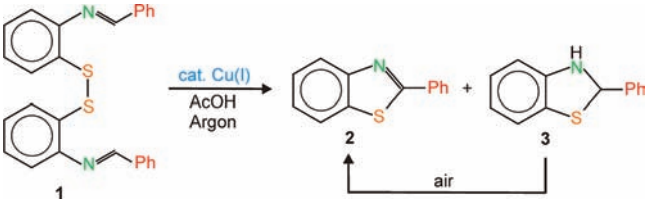

bond and formation of the C−S bond accompanied by hydrogen transfer as a direct route to the products. In this way, the formation of high-valent copper species as supposedly unstable intermediates can be circumvented. Related reactions have indeed been observed for metal-coordinated S_2^{2-} moieties.[26] Further, it is useful to refer to the chemistry of the related peroxides, for which various mechanistic variants other than oxidative addition are known, such as homolytic cleavages or acid-catalyzed rearrangements,[27] and even simple protonation can trigger the cleavage of the O−O bonds of peroxides.[28]

In order to unravel the key factors for the present carbon−heteroatom bond formation by copper catalysis and thereby explore the nature of the interaction between the metal and the disulfide fragment, we report a combined experimental and theoretical investigation of the process shown in Scheme 1 for the imine disulfide parent compound **1** in the gas phase. Thereby, the previous exploratory experimental studies[2] are completed as well as extended, providing a consistent mechanistic view of the title reaction.

EXPERIMENTAL DETAILS

The experiments were performed using Finnigan LCQ Classic ion-trap mass spectrometer (IT-MS)[29] by ESI of dilute methanol solutions of the reactant **1** and the catalyst [copper(I) 3-methylsalicylate]. In brief, the LCQ bears a conventional ESI source consisting of the spray unit (typical flow rates range between 5 and 30 μL/min; typical spray voltage is 5 kV) with nitrogen as a sheath gas, followed by a heated transfer capillary (kept at 200 °C), a first set of lenses which determines the soft- or hardness of ionization by variation of the degree of collisional activation in the medium pressure regime,[30,31] two transfer octopoles, and a Paul ion trap with ca. 10^{-3} mbar helium for ion storage and manipulation, including a variety of MS^n experiments.[32] For detection, the ions are ejected from the trap to an electron multiplier. Low-energy collision-induced dissociation (CID) was performed by application of an excitation ac voltage to the end-caps of the trap to induce collisions of the kinetically excited ions with the helium buffer gas.[33] For a CID excitation period of 20 ms and a trapping parameter of $q_z = 0.25$, we have recently introduced an empirical calibration scheme that allows a conversion of the experimental appearance energies (AEs) of the fragmentations to an absolute energy scale.[34] The respective determinations of the AEs were performed twice, and the results shown here are the averages of the two data sets. In between both measurements, the correctness of the phenomenological calibration factor used was checked by CID of mass-selected benzylpyridinium ions.[34b]

Gas-phase infrared spectra (IR) of the mass-selected complex **1**/Cu^+ (m/z 487 for the ^{63}Cu isotope) and that of the putative copper complex of the dihydrobenzothiazole product with one additional water (m/z 294 for the ^{63}Cu isotope) were recorded with a Bruker Esquire 3000 IT-MS[35−37] mounted to a beamline of the free electron laser at CLIO (Centre Laser Infrarouge Orsay, Orsay, France). The ions of interest were generated by ESI and then transferred to the ion trap. After mass selection, infrared multiphoton dissociation was induced by admittance of four macropulses of IR-laser light to the ion trap. Monitoring the abundances of the fragment ions formed as a function of the wavelength provides IR spectra of the mass-selected ions. Because the fragmentation thresholds of the ions are much above the energy of a single IR photon in the spectral regime covered, several photons are required to bring about dissociation. Accordingly, the experiments are commonly referred to as infrared-multiphoton dissociation (IRMPD);[38] note, however, that the process involves the sequential absorption of several photons, not the simultaneous action of multiple photons. In the 45 MeV range in which CLIO was operated during these experiments, the IR light covers a spectral range from about 1000 to about 2000 cm^{-1}. One data point of a typical IRMPD spectrum is derived from the average of four mass spectra (each with eight accumulated microscans) per wavelength, then the latter is changed with a step size of about 5 cm^{-1} and the next data point is taken. The typical acquisition time of an IRMPD spectra spanning a spectral range of ca. 1000 cm^{-1} is about an hour. Due to occasional instabilities of the combination of the IR laser and ESI-MS, all spectra at CLIO were at least taken two times, and the data shown below are the averages of these runs.

COMPUTATIONAL METHODS

Quantum chemical calculations were performed using the hybrid density functional method B3LYP-D, which includes an empirical treatment for dispersion (its revision 2).[39,40] Unless stated otherwise, the results discussed below refer to singlet multiplicity. Several investigated species were found to have diradical character, whose singlet state can only be treated approximately within single-configurational Kohn−Sham DFT, using the broken-symmetry approach,[41,42] i.e., unrestricted calculations with $S_z = 0$. With the typical functionals, this procedure yields spin contamination in the Kohn−Sham wave functions, and schemes have been suggested for obtaining corrected energies,[41−43] geometries,[44,45] and frequencies.[46] However, there is an ongoing discussion whether these corrections are theoretically sound and improve the results practically, because $\langle S^2 \rangle$ of the reference noninteracting wave function may not be a correct measure of spin contamination, and the symmetry breaking can actually account for some static correlation effects;[47−49] moreover, the first derivatives of energy become discontinuous upon applying spin projection.[50] Unless explicitly noted, we present geometries and energetics from uncorrected (spin contaminated), unrestricted calculations. We calculated single-point B3LYP-D spin-projected singlet energies using the Yamaguchi formula[43] at all stationary points and found that the approximate projection has only minor influence on energies; importantly, none of our conclusions would be affected. The spin-projected energies, together with all $\langle S^2 \rangle$ values, are reported in the Supporting Information.

The def2-SVP basis set was used for geometry optimization, harmonic vibrational frequency calculation, and electronic structure analysis, whereas the def2-TZVPP was employed for the determination of the final single-point energies.[51] The latter calculations were carried out using the resolution of identity approximation.[52] Additional single-point calculations at the M06/def2-TZVPP level,[53] provided in the Supporting Information, indicate that the main conclusions made below are independent of the specific functional chosen. The closed-shell or open-shell nature of the M06 Kohn-Sham determinants and their $\langle S^2 \rangle$ values also correlate well with the B3LYP-D results.

All structures reported below are either minima or first-order saddle points on the potential-energy surface, respectively, as revealed by analysis of the corresponding Hessian matrices. All transition structures were checked for connecting the anticipated minima by inspection of the transitional normal mode and starting optimizations from structures displaced along it. Values of the imaginary frequencies

of the transitional modes are provided in the Supporting Information. For some structures, single, very small imaginary frequencies (<25i cm^{-1}) associated with collective modes remained after optimization; however, these are not expected to significantly affect the computed energetics. In several cases, multiple conformers of the involved species were identified. The calculations revealed that the associated conformational transitions have significantly lower barriers than the actual bond formations or cleavages; we therefore treat these conformers as a common ensemble and only discuss the most stable structures found.

The computed energies given below correspond to zero-point vibrational energy corrected electronic energies; all calculations refer to the gaseous state in that additional solvation, aggregation, and other similar effects are deliberately not included. For comparison with the experimental infrared spectra, in agreement with common practice, we use a uniform scaling factor for the calculated harmonic frequencies. On the basis of experience on similarly sized double-ζ basis sets, we employed a factor of 0.97 throughout.[54] Previous IRMPD studies of related 3d transition-metal complexes have amply justified the use of scaling.[7b,38d,55] For the sake of simplicity, we utilized the same scaling factor also in the computation of the zero-point vibrational energies. Modeling of infrared spectra was done using a Gaussian line shape with a full peak width at half-maximum of 20 cm^{-1}, chosen to match the experimental spectra by their appearance.

The computations were mostly carried out with the Turbomole software package;[56] M06 tests were done using Gaussian 09.[57] Molecular graphics were drawn using Molekel.[58]

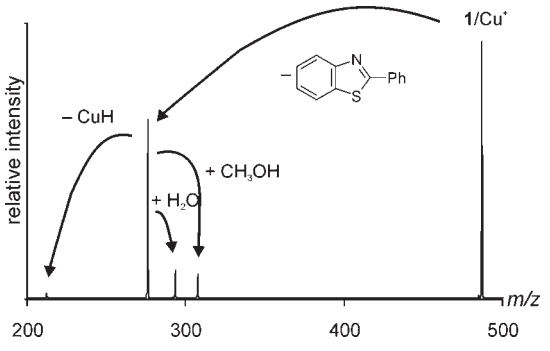

Figure 1. Fragmentation of mass-selected **1**/Cu^+ (m/z 487 for ^{63}Cu) in the gas phase.

RESULTS AND DISCUSSION

The present work aims toward a detailed analysis of the gas-phase fragmentation of the complex **1**/Cu^+ between the parent imine disulfide **1** and an atomic copper cation. Figure 1 shows the collision-induced dissociation (CID) mass spectrum of **1**/Cu^+ (m/z 487 for the ^{63}Cu isotope) with a product ion with m/z 276 as major fragment, which formally corresponds to the complex of product **3** with Cu^+, while 2-phenylbenzothiazole (**2**) is lost as a neutral fragment.[2] Hence, the interaction of the substrate with a single copper cation in the gas phase can bring about the same products as observed in the preparative reaction in solution (Scheme 1). At elevated collision energies, the primary fragment ion with m/z 276 undergoes further dissociation to afford an ion with m/z 212 concomitant with a loss of neutral CuH. Figure 1 also shows signals at m/z 294 and 308, which can be assigned to additions of water and methanol, respectively, present in the background of the vacuum system of the IT-MS (see also below).[34a]

Computational Analysis of the Parent Ion. In order to interpret the structure of the parent ion and follow its isomerization pathways leading to the experimentally observed fragmentations, we have first explored computationally the potential-energy surface (PES) associated with the reactant complex **1**/Cu^+ and its possible rearranged structures (all having m/z 487). Because the loss of 2-phenylbenzothiazole (**2**) is observed experimentally, we particularly aim to find transformations that yield copper species containing **2** as a separate ligand.

As the starting point of the gas-phase reaction and the reference of the relative energy scale, we have chosen the Cu^+ adduct of **1**, hereafter referred to as reactant complex **A** (Figure 2).[59] In the closed-shell singlet species **A**, both sulfur and both nitrogen atoms of **1** form dative bonds toward the copper, providing a coordination environment with distorted seesaw geometry. The tetradentate ligand **1** has a total binding energy to Cu^+ of 123.8 kcal mol^{-1}. The sulfur–sulfur bond is retained in **1**/Cu^+ but slightly elongated (2.24 Å) as compared to the free ligand (2.18 Å); the phenyl groups on the imine carbons are in a displaced parallel stacked arrangement. The computed Mulliken d orbital population of 9.73 on copper is consistent with the notion of a Cu(I) complex.

The conceivable rearrangements of the reactant complex **A** as revealed by the computations are summarized in Figure 3 in the

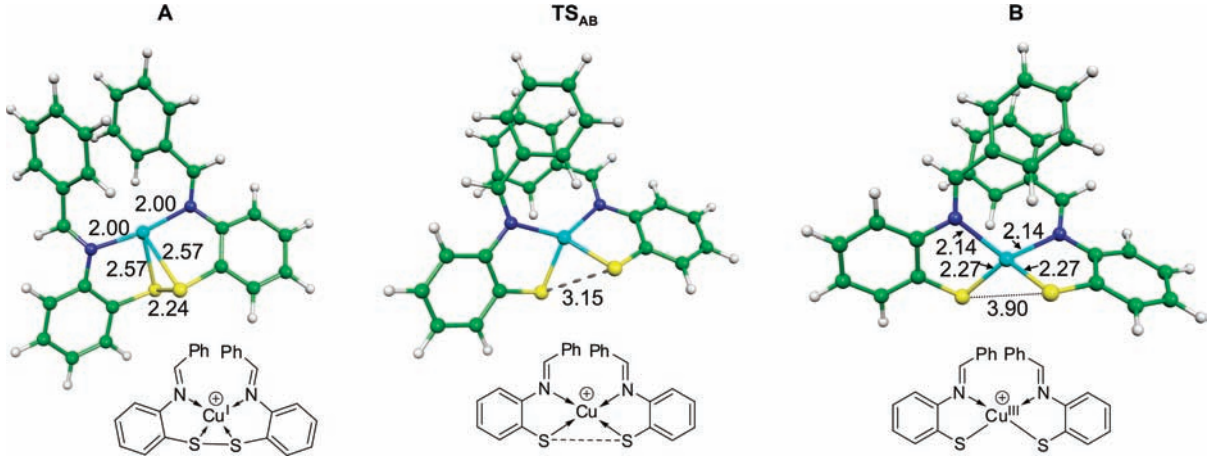

Figure 2. Optimized structure of the reactant complex **A** (i.e., the simple adduct of **1** and Cu^+) and the stationary points along the sulfur–sulfur oxidative addition. Atom color code: Cu, turqoise; N, dark blue; S, yellow; C, green; H, white. Distances are in Å.

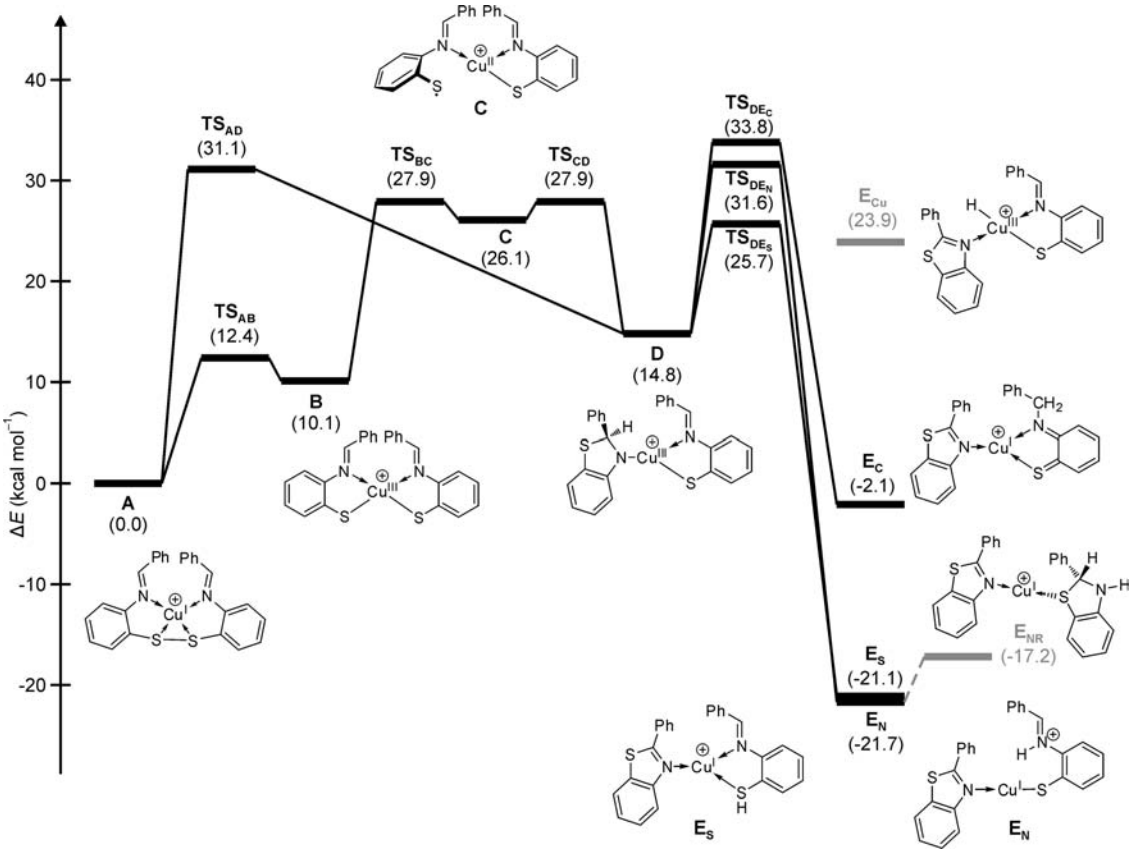

Figure 3. Calculated energy profile for the possible transformations of the reactant complex **A**. Note that the pathways leading to $\mathbf{E_{Cu}}$ and $\mathbf{E_{NR}}$ were not determined.

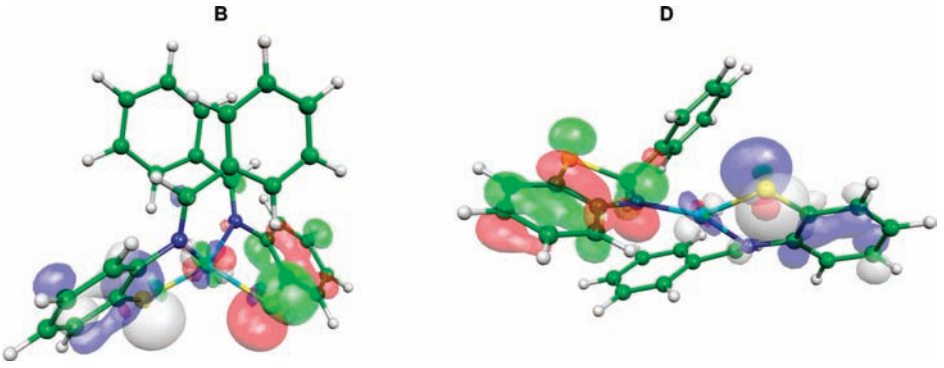

Figure 4. Pair of magnetic orbitals of the copper(III) disulfide intermediate (**B**) and of the heterocyclic copper(III) intermediate (**D**). The α orbital is colored blue−white, and the β orbital is shown in red−green.

form of an energy diagram. From the reactant complex **A**, a formal oxidative addition of copper into the S−S bond can proceed easily on the singlet PES, through transition structure $\mathbf{TS_{AB}}$ associated with an activation energy of 12.4 kcal mol^{-1} (Figure 2). The resulting copper(III) disulfide intermediate **B** has a fully cleaved S−S bond (3.90 Å) and is 10.1 kcal mol^{-1} higher in energy than **A**. The copper in structure **B** remains four-coordinate, but the coordination geometry around it is converted to a distorted tetrahedron.

At the B3LYP-D level of theory, the copper(III) disulfide **B** has a diradical character, the triplet state being 1.1 kcal mol^{-1} more stable than the open-shell singlet. In order to get further insight into the electronic structure, we applied the corresponding orbital transformation[60] on the broken-symmetry singlet wave function, which showed the presence of a single pair of interacting magnetic orbitals (Figure 4).

The low-lying and compact d orbitals of copper interact only weakly with the sulfur p orbitals, and therefore, these magnetic orbitals mostly correspond to unpaired electrons on sulfur atoms, with some Cu−S antibonding character and an appreciable delocalization to the phenyl rings. Due to the peculiar nonplanar geometry of the complex, together with the half-twisted C−S−Cu−S−C moiety, the two orbitals are essentially orthogonal (their overlap integral is 0.0075), which explains the

dx.doi.org/10.1021/ic200442s |*Inorg. Chem.* 2011, 50, 9968–9979

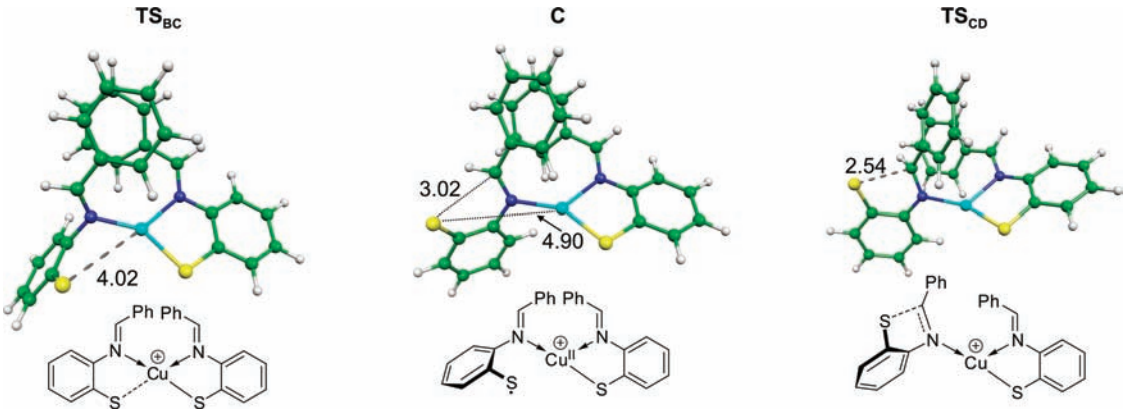

Figure 5. Stationary points along the stepwise ring-closing pathway.

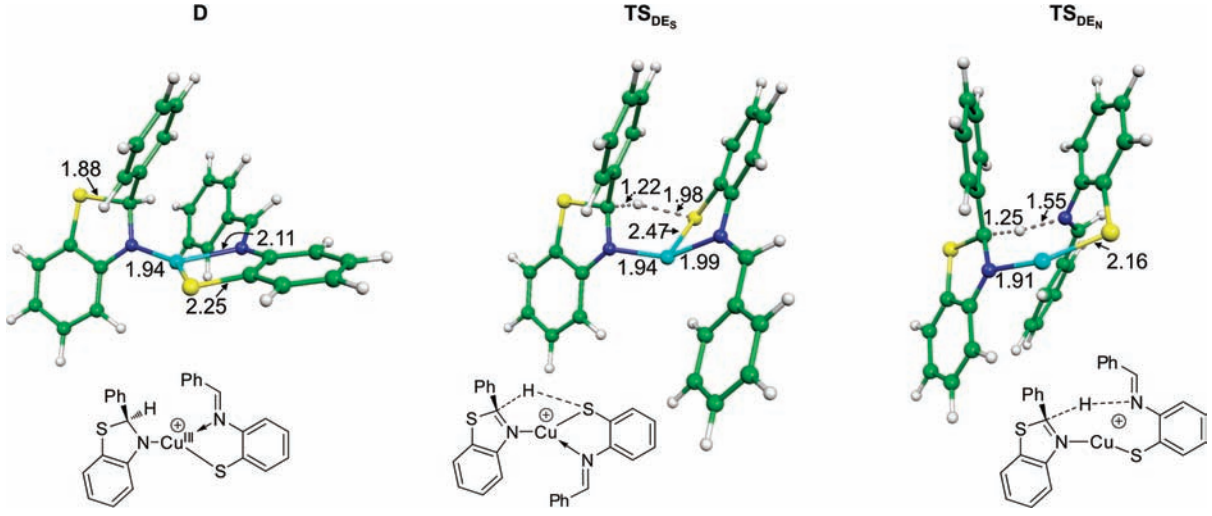

Figure 6. Optimized structure of the heterocyclic copper(III) intermediate **D** and the transition structures for its further transformation to the products. In the case of $\mathbf{TS}_{\mathbf{DE}_S}$, a conformational change involving rotation of the two ligands with respect to each other (around the left Cu−N bond) is necessary to arrive at $\mathbf{TS}_{\mathbf{DE}_S}$ (from **D**). For $\mathbf{TS}_{\mathbf{DE}_N}$, the copper−nitrogen dative bond of the right-hand side ligand is broken along the way to the transition structure.

computed ferromagnetic coupling between them. The presence of mainly ligand-centered radical sites and the Mulliken *d* orbital population on copper of 9.60 imply that this formal Cu(III) disulfide species has notable Cu(I) dithiyl character.[61,62]

Starting from the complex **B**, a two-step process may lead to the closing of the heterocyclic ring for one "half" of the reactant molecule **1** (Figure 5). One of the Cu−S bonds is broken first ($\mathbf{TS}_{\mathbf{BC}}$, 27.9 kcal mol^{-1}), leaving behind a three-coordinate Cu(II) and yielding the unstable intermediate **C** (the calculated d electron population is 9.68). From **C**, a rotation of the phenyl group bearing the free sulfur radical allows the attack of the imine carbon concomitant with the formation of a C−S bond ($\mathbf{TS}_{\mathbf{CD}}$, 27.9 kcal mol^{-1}).

The product of this stepwise process is the heterocyclic copper(III) intermediate **D** (Figure 6), which is 14.8 kcal mol^{-1} above the reactant complex **A**. Similarly to the copper(III) disulfide intermediate **B**, this species has a diradical character; in this case, the open-shell singlet state lying somewhat below the triplet (ΔE = 1.2 kcal mol^{-1}). Application of the corresponding orbital transformation to the broken-symmetry singlet wave function again yields a single pair of magnetic orbitals for **D**, as shown in Figure 4. These orbitals are essentially ligand-centered, and in this case, there is a significant overlap between them (consider the lobes on Cu and the sulfur on the right-hand side; the overlap integral is 0.3807), which accounts for the antiferromagnetic interaction. The orbital shapes and the Mulliken d orbital population on Cu of 9.64 support a character of two copper(I) bound radicals in this case as well.

Interestingly, the reactant complex **A** can also react to yield the above-discussed heterocyclic Cu(III) intermediate **D** in a single step via $\mathbf{TS}_{\mathbf{AD}}$ (Figure 7). In this multiply centered transition structure, several bonds are cleaved and formed in a single elementary process. Namely, one of the sulfur atoms breaks its bonds toward the copper and the other sulfur and simultaneously attacks the imine carbon atom, directly yielding the heterocyclic ring. The computed barrier for this pathway (31.1 kcal mol^{-1}) is only modestly higher than that of the stepwise process, and the M06 functional even predicts this concerted route to be preferred.

We can now arrive at a product complex, containing a separate 2-phenylbenzothiazole (**2**) coordinated to copper, if

dx.doi.org/10.1021/ic200442s |*Inorg. Chem.* 2011, 50, 9968–9979

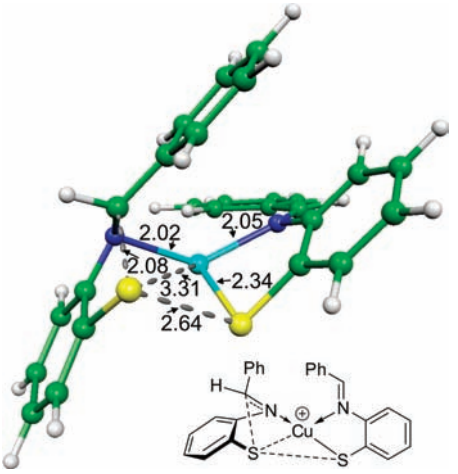

Figure 7. Transition structure $\mathbf{TS_{AD}}$ leading directly from **A** to **D**.

the hydrogen atom is abstracted from the newly created ring in the heterocyclic copper(III) intermediate **D**. Several pathways for hydrogen transfer can be envisioned, differing in the target atom accepting the hydrogen. Computations show that the kinetically preferred way is to transfer this hydrogen atom to the sulfur of the other ligand ($\mathbf{TS_{DE_S}}$, Figure 6), with a computed barrier of 25.7 kcal mol^{-1}, producing product isomer $\mathbf{E_S}$ that has an imine thiol ligand apart from the benzothiazole. The thermodynamically favored pathway corresponds to a hydrogen transfer to the nitrogen ($\mathbf{TS_{DE_N}}$, 31.6 kcal mol^{-1}, Figure 6), which yields product $\mathbf{E_N}$, in which an iminium thiolate and a benzothiazole ligand are coordinated to copper. Hydrogen-atom transfer to the carbon is neither kinetically nor thermodynamically favorable; hydrogen transfer to copper can be already excluded on the basis of the high energy of the supposed product $\mathbf{E_{Cu}}$ (Figure 3).

Disregarding the improbable $\mathbf{E_{Cu}}$ form, all resulting isomers of product complex **E** are again closed-shell singlet Cu(I) species (d orbital populations are greater than 9.6 for all of them), which means that the hydrogen transfer between the two ligands is coupled with a formal reduction from Cu(III) to Cu(I). In the light of our above findings about the electronic structures of the involved copper(III) intermediates, however, these reactions can be thought of as radical quenching by hydrogen atom abstraction. Furthermore, a ring closure of the reduced ligand to dihydrobenzothiazole is considered. The most stable structure of this type of bisligated copper complex, $\mathbf{E_{NR}}$, is higher in energy than the open forms by ~4 kcal mol^{-1}; the dihydrobenzothiazole moiety is bound via its sulfur atom.[63] From any of these product complexes ($\mathbf{E_S}$, $\mathbf{E_N}$, $\mathbf{E_C}$, $\mathbf{E_{NR}}$), 2-phenylbenzothiazole (**2**) can be released via direct ligand loss.

We have also attempted to find further alternative routes from reactant complex **A** to the **E**-type product isomers, but all other located pathways involve barriers higher than those of the routes discussed above. Notably, we were not able to find any mechanisms that would avoid the formation of formal copper(III) species (see also the Supporting Information).

Computational Analysis of the Fragmentation. From the product complexes **E** containing the 2-phenylbenzothiazole unit, the first fragmentation step leads to the ion with m/z 276, which corresponds to the loss of neutral **2**. For the resulting fragment ion, several structures based upon a monocyclic ligand backbone (i.e., $\mathbf{F_S}$, $\mathbf{F_N}$, and $\mathbf{F_C}$) as well as a structure with a closed dihydrobenzothiazole ring ($\mathbf{F_{NR}}$) can be envisaged, which are related to the dissociation of the respective isomers of the product complex **E** and are all copper(I) species (Figure 8).[64] Energetically, there is a clear preference for the formation of $\mathbf{F_S}$ + **2** which is only 25.4 kcal mol^{-1} endothermic with respect to **A**. However, note that along the pathway the barrier associated with the formation of $\mathbf{E_S}$ needs to be crossed (27.9 kcal mol^{-1}). The relative stabilities of the isomers $\mathbf{F_C}$ and $\mathbf{F_S}$ parallel those of the corresponding isomers of **E**. In contrast, $\mathbf{F_N}$ is markedly less stable than $\mathbf{F_S}$ and also $\mathbf{F_{NR}}$ is increasingly disfavored. In both cases, the effect may be attributed to the presence of only a single electron-donating heteroatom coordinating the copper atom, hence leading to a destabilization.[8]

The second fragmentation step, corresponding to the loss of CuH from the **F** isomers, is of no importance with respect to the catalyzed title reaction and the role of copper; its computational analysis is therefore provided only in the Supporting Information. We note, however, that the fragment ion with m/z 212 formed upon loss of CuH can be safely assigned as protonated 2-phenylbenzothiazole ($\mathbf{2}-H^+$). En route to the fragmentation into $\mathbf{2}-H^+$ + CuH, the passage of one of the TSs has the highest energy demand, 40.1 kcal mol^{-1}, relative to the most stable structure $\mathbf{F_S}$ of the ion with m/z 276, while the overall endothermicity is 33.9 kcal mol^{-1} relative to $\mathbf{F_S}$.

Structural Assignment of the Parent Ion with *m/z* 487. Having the computed energy landscape at hand, we turned to experiments to probe the structure of the observed precursor ion with m/z 487 and to determine which point on the PES it may correspond to: is it the mere adduct of **1** and Cu^+ (i.e., reactant complex **A**), some product complex ($\mathbf{E_S}$, $\mathbf{E_N}$, or $\mathbf{E_{NR}}$), or a different isomer? First, we investigated if this species contains exchangeable protons, as would be expected if it had a product-like structure such as the **E**-isomers. To this end, reactant **1** and the copper catalyst were dissolved in CH_3OH and CD_3OD, respectively, and analyzed via ESI-MS. In the instrument used, part of the solvent used in ESI inevitably diffuses into the mass analyzer, and exchangeable positions are hence expected to give rise to H/D exchange. On the other hand, even if occurring, the exchange is only partial, because of additional moisture present in the ion trap from previous experiments with protic solvents, even after treating for several hours with CD_3OD.[29,65] Figure 9 depicts the isotope envelopes measured in the respective experiments as well as the patterns calculated for the corresponding natural isotopic distributions. In the case of the precursor ion (Figure 9a), the three traces match quite well, indicating that no H/D exchange takes place. In contrast, the two fragment ions (m/z 276 and 212) show increased abundances of the ions at m/z 277 and 213, respectively, in the measurements conducted using CD_3OD, indicating the occurrence of H/D exchange in the gas phase[66] to yield the respective deuterated species. Taking these observations together, it seems justified to conclude that the precursor ion is not converted spontaneously to $\mathbf{E_S}$-, $\mathbf{E_N}$-, or $\mathbf{E_{NR}}$-type isomers of the product complexes.

As a further probe, we recorded the gas-phase infrared spectrum of the mass-selected precursor ion to obtain structural information. The IRMPD spectrum of the ion at m/z 487 (Figure 10) shows an intense band at about 1600 cm^{-1} with a shoulder at around 1570 cm^{-1} and another weak band at ~1460 cm^{-1}.[67] The major bands in the measured spectrum are in good agreement with the (scaled) computed peak positions for reactant complex **A**. With respect to intensities, we note that due to the multiphotonic nature of the IRMPD experiments the amount of ion fragmentation is not always proportional to the

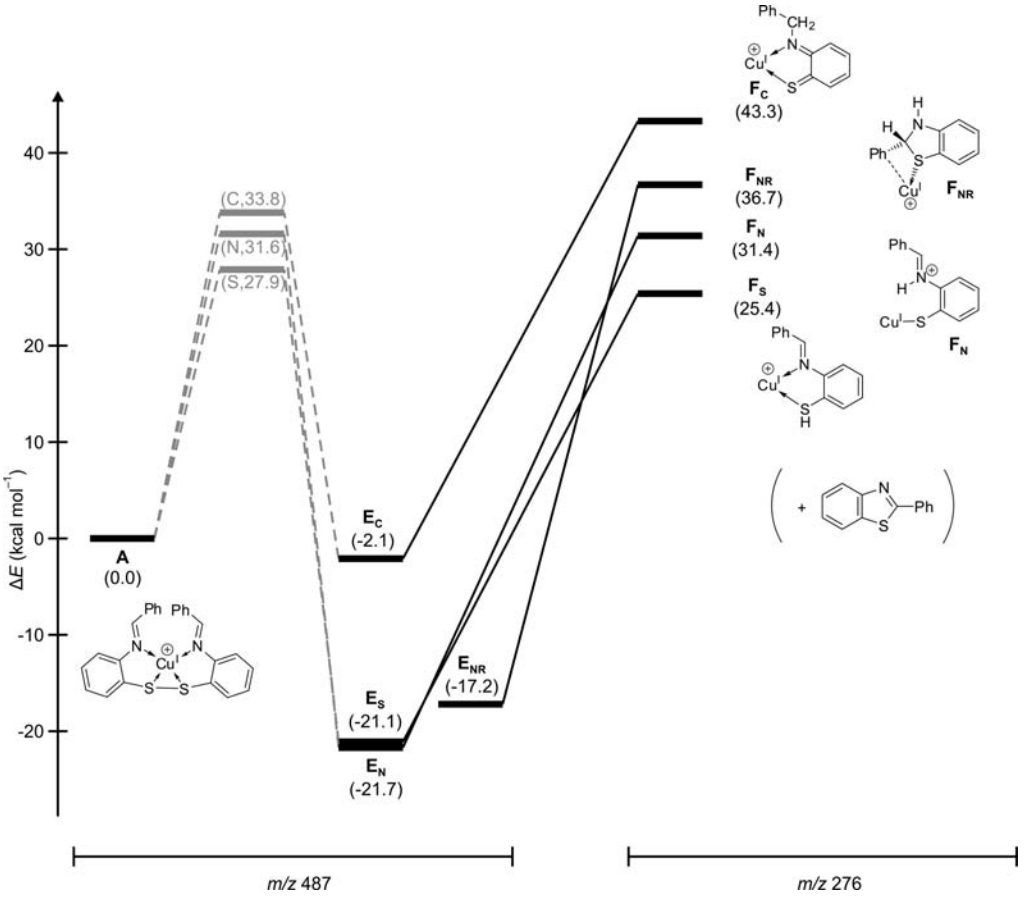

Figure 8. Computed energy profiles for the loss of phenylbenzothiazole **2** to form the ions **F** (m/z 276). The pathway between the reactant complex **A** and product complexes **E** is shown in Figure 3 and hence only the largest barriers are shown here.

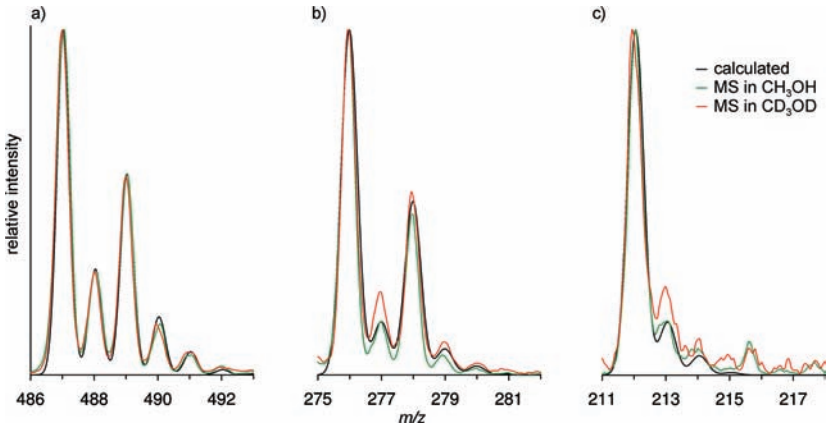

Figure 9. Calculated and measured isotope pattern of the precursor ion (m/z 487, a) and of the two fragment ions after neutral benzothiazole loss (m/z 276, b) and subsequent CuH loss (m/z 212, c). The data were scaled to have the same intensity of the base peaks in the respective mass region. Note the good agreement of all curves for m/z 488 in part a, whereas the corresponding peaks at m/z 277 and 213, respectively, increase in abundance in the experiments with CD_3OD (b and c).

(single photon) IR absorbance; the major weight is therefore put on the peak positions, rather than the peak heights in the IRMPD spectra.[68,69] In agreement with intuitive assignments based on typical infrared patterns in organic structural analysis, computations predict the two largest bands (1603 and 1563 cm^{-1}) to stem from normal modes corresponding to various combinations of C═N and aromatic C−C stretching vibrations (10 modes altogether), whereas the third largest computed peak (1443 cm^{-1}) originates from aromatic C−H in-plane bending motions.

While the computed IR spectra of the product complexes $\mathbf{E_C}$ and $\mathbf{E_{NR}}$ are quite different and the presence of these isomers can thus be excluded, those of **D**, $\mathbf{E_N}$, and $\mathbf{E_S}$ are in moderate agreement and that of **B** fits the experimental spectrum similarly well as **A** (**C** was not considered at all; see the Supporting

dx.doi.org/10.1021/ic200442s |*Inorg. Chem.* 2011, 50, 9968–9979

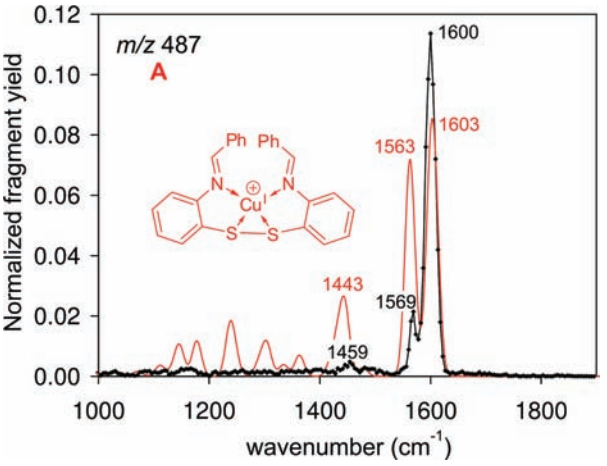

Figure 10. Experimental IRMPD spectrum of $\mathbf{1}/Cu^+$ (m/z 487, black) and computed IR spectrum of reactant complex **A** (red; overall intensity arbitrarily scaled) in the range from 1000 to 1900 cm^{-1}. The numbers indicate the positions of the maxima.

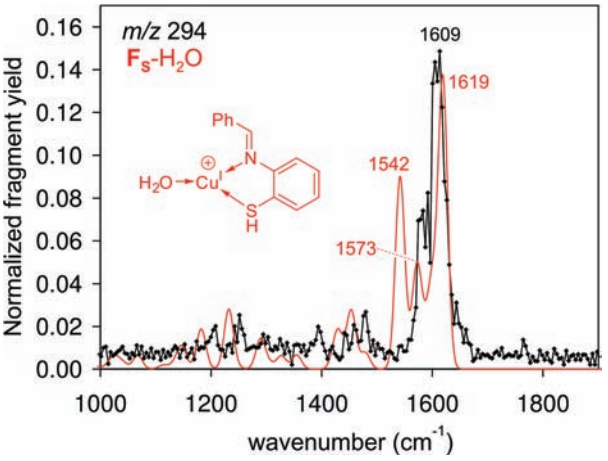

Figure 11. Experimental IRMPD spectrum of fragment ion formed by benzothiazole loss and water uptake (m/z 294, black) and computed IR spectrum of $\mathbf{F_S}-H_2O$ (overall intensity arbitrarily scaled, red) in the range from 1000 to 1900 cm^{-1}. The numbers indicate the positions of the maxima.

Information). Therefore, the IRMPD results alone are not sufficient to provide an unambiguous assignment of the ion structure. However, $\mathbf{E_S}$ and $\mathbf{E_N}$ bear exchangeable protons and are hence expected to undergo H/D exchange, which contradicts the results shown in Figure 9a. While structure **B**, the product of oxidative addition, cannot be excluded strictly, it is computed to be significantly higher in energy than **A**, and the reverse activation barrier is rather small (Figure 3), such that its contribution to the gross population of m/z 487 is assumed to be negligible. The same holds for **D**, which is even less stable, and the barrier for its transformation to products is smaller than for its production. Collecting all the information obtained, we may conclude that the precursor ion with m/z 487 corresponds to structure **A**, and accordingly, the stepwise rearrangement shown in Figure 3 only takes place in the course of ion excitation and subsequent dissociation. However, it is emphasized that this assignment of structure **A** to the ion with m/z 487 is partially based on the computed relative energetics of the isomers.

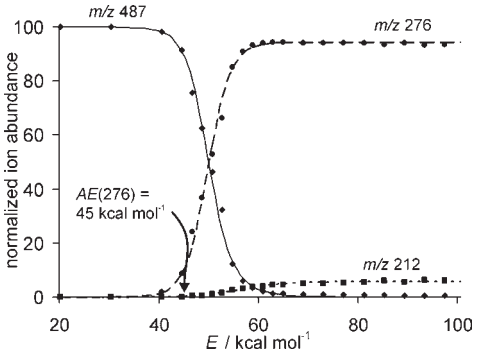

Figure 12. CID breakdown diagram of $\mathbf{1}/Cu^+$ (m/z 487) to afford fragments with m/z 276 and 212. Two additional minor channels appear at m/z 294 and 308 (Figure 1) and are assigned to subsequent additions of water and methanol, respectively, to the product ion at m/z 276; these neutral reagents are residuals from the spray solvent, and water is also present in the background of the mass spectrometer. The abundances of these species were accordingly added to that of m/z 276.

Structural Assignment of the First Fragment Ion with *m/z* 276. An experimental structural characterization of the product of 2-phenylbenzothiazole loss at m/z 276 was again attempted using H/D exchange and IRMPD measurements. As demonstrated in Figure 9b, the experiments provide evidence for the presence of exchangeable protons in this ion, which is a strong argument against structure $\mathbf{F_C}$. Direct IRMPD measurements of m/z 276 were not feasible because the IR photons were not able to induce a sufficient amount of fragmentation in the competition with a rapid adduct formation with background water. We took advantage of the latter and deliberately studied the water adduct (m/z 294) instead, for which the IR photons can easily bring about the loss of a water molecule. The experimental spectrum shown in Figure 11 is similar to that of the parent ion, but upon closer look, we can identify a blue-shift of approximately ~10 cm^{-1} of the most intense absorption. In the computed spectrum of the most probable isomer $\mathbf{F_S}-H_2O$, the largest peak (1619 cm^{-1}) stems from an almost pure C═N stretching mode, while four aromatic C−C stretching vibrations with slight mixing of C═N stretch contribute to a shoulder on its left (~1600 cm^{-1}) and to the third largest peak (1573 cm^{-1}). The computationally second most intense transition (1542 cm^{-1}) corresponds to an O−H in-plane bending of the water ligand.[70] The computed spectrum in general fits well the experiment, reproducing the shift in the most intense C═N stretching mode, while the O−H bending at 1542 cm^{-1} seems to appear within the multiplet between 1570 and 1620 cm^{-1} in the experimental IRMPD spectrum. Similarly to the ambiguity encountered in the case of m/z 487, the measured spectrum for m/z 294 is also in moderate agreement with the calculations for $\mathbf{F_N}-H_2O$, which is higher in energy, however. Instead, the structures $\mathbf{F_C}$ and $\mathbf{F_{NR}}$ can be safely excluded due to their different IR patterns (see the Supporting Information). Again, only a combination of the available experimental and computational information allows an assignment of the ion with m/z 276, yielding structure $\mathbf{F_S}$ as the most likely candidate. As to the secondary fragment with m/z 212, we only note that the observation of exchangeable protons (Figure 9c) is in accordance with the suggested structure of protonated 2-phenylbenzothiazole.

Energy Demand for the Dissociation of $1/Cu^+$. The experimentally observed energy dependence of the collision-induced dissociation of the mass-selected ion **A** to yield the fragment ion

dx.doi.org/10.1021/ic200442s |Inorg. Chem. 2011, 50, 9968–9979

Table 1. Summarized Results of CID Experiments of Mass-Selected Cations 1/M$^+$ with Various Cations M$^+$

M$^+$	m/z[a]	AE[b]	radical loss[c]
H^+	425	45	–
Li^+	431	55	+
Na^+	447	62	+
$NiCl^+$	517	43	–
Cu^+	487	45	–
$ZnCl^+$	523	45	–
Ag^+	531	44	–

[a] Mass-to-charge ratio of the corresponding **1**/M$^+$ complexes given for the leading isotopes. [b] Appearance energies (in kcal mol^{-1}) derived from modeling the breakdown graph using a sigmoid function; error, ±10%. [c] Occurrence (+) or nonoccurrence (–) of direct S–S bond cleavage concomitant with loss of the corresponding thiyl radical.

at m/z 276 is shown in Figure 12. By reference to a calibration-based method,[34] the apparent threshold of the benzothiazole loss amounts to 45 ± 5 kcal mol^{-1}. Theory predicts the highest barrier en route to the products to be only 27.9 kcal mol^{-1} (Figures 3 and 8). Despite several sources of systematic errors in both experiment and theory, we assign the major source of the divergence to the operation of a kinetic shift in ion dissociation.[71] Thus, the empirical calibration of the energy scale in the IT-MS measurements[34] is referenced to direct bond cleavages, which proceed as continuously endothermic processes without a barrier in excess of the reaction endothermicity. Instead, the computational survey of the title reaction demonstrates its occurrence as a complex structural rearrangement, and hence it is indeed quite likely to require additional excess energy to proceed under the experimental conditions. In fact, kinetic shifts having the magnitude as observed here are not unexpected in general[71,72] and have been reported for transition-metal complexes.[73] However, a reliable theoretical prediction of the kinetic shift would require a precise knowledge of the energy-transfer processes occurring in the ion trap as well as a formidable computational effort for the treatment of a multistep reaction of complex molecules, which is far beyond the scope of this paper.

Mediation of S–S Bond Cleavage in 1 by Other Metal Ions. In the preparative experiments in solution, a blank experiment in acetic acid without addition of metal catalysts gave no conversion under typical conditions, whereas replacement of the copper(I) catalyst by either ruthenium or palladium complexes afforded the desired products, but the reactions were more sluggish and the yields were lower. In the gas phase, it might be possible that the S–S bond cleavage in **1** is also induced by other metals, including those not being able to undergo oxidative addition. Accordingly, we probed this alternative by subjecting complexes of several other cations M$^+$ with neutral **1** to CID experiments. Table 1 provides a general overview of the results obtained for various cationic complexes; the complete details are given in the Supporting Information.

Upon CID, all **1**/M$^+$ complexes studied undergo S–S bond cleavage concomitant with the release of neutral benzothiazole (see the Supporting Information). In the gas phase, the title reaction thus is not specific for copper but can also be mediated by other metals and even by a proton. Moreover, most of the measured appearance energies match the value of 45 ± 5 kcal mol^{-1} found for M$^+$ = Cu$^+$. Only for M = Li and Na, the apperance energies are slightly larger, and the dissociations are

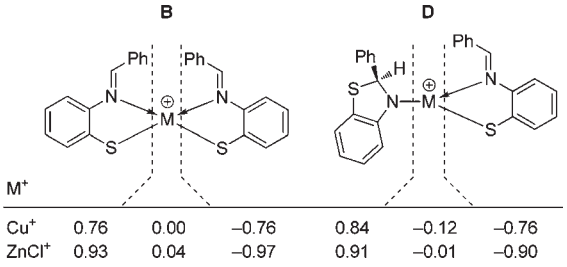

Figure 13. Open-shell singlet Mulliken spin populations of the structures **B** and **D** for M = Cu and ZnCl, respectively, summed up for the cations and ligands as indicated. Note that the values on the ligands are significantly closer to ±1 in the case of zinc, indicating a larger diradical character and the absence of the involvement of a higher oxidation state.

Scheme 2. Conceivable Pathways for the S–S Bond Cleavage by a Cation M$^+$: (a) S–S Bond Homolysis to Yield a Radical Pair, (b) Oxidative Addition of the Metal into the S–S Bond, and (c) S–S Bond Heterolysis by Lewis Acid Catalysis to Yield a Transient Sulfur-Centered Cation Bound to a Neutral Metal Thiolate

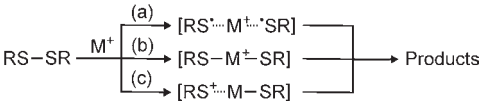

accompanied by competing losses of thiyl radicals corresponding to direct S–S bond cleavages. While the S–S bond homolysis only requires 48.0 kcal mol^{-1} in the free ligand, expulsion of a thiyl radical from the Cu$^+$-containing reactant complex **A** was calculated to be endothermic by 77.1 kcal mol^{-1}. This value strongly suggests that a mechanism based on direct S–S cleavage and radical roaming is only competitive at higher energies. Accordingly, the results in Table 1 suggest the existence of additional mechanistic pathways of the title reaction.

One of these pathways involves oxidative addition as revealed by the extensive calculations for the copper systems (see above). While one might invoke similar routes for nickel and silver, oxidative addition via high-valent intermediates can safely be excluded for zinc, the two alkali metals, and the proton. To understand the behavior in this class better, we carried out exploratory computations on zinc. For the ZnCl$^+$-catalyzed reaction, we identified a full reaction pathway for the benzothiazole loss that is analogous to the concerted **A**–**TS$_{AD}$**–**D**–**TS$_{DE_S}$**–**E$_S$**–**F$_S$** route for copper. The highest point along this route is ZnCl$^+$–**TS$_{AD}$**, which is 31.2 kcal mol^{-1} above the reactant complex ZnCl$^+$–**A**, while the key intermediate ZnCl$^+$–**D** is at 17.4 kcal mol^{-1} with respect to the same reference. Both values are quite close to their copper counterparts (31.1 and 14.8 kcal mol^{-1}), respectively. On the other hand, ZnCl$^+$-containing species that correspond to intermediates along the stepwise, oxidative addition-based route **A**–**B**–**C**–**D** are indeed much less stable; i.e., ZnCl$^+$–**B** and ZnCl$^+$–**C** lie at 30.0 and 33.7 kcal mol^{-1} compared to values of 10.1 and 26.1 kcal mol^{-1} for copper, respectively. These theoretical results, along with the difference in the electronic structures between the Cu$^+$ and ZnCl$^+$ variants of **B**/**D** (Figure 13), imply a clear mechanistic difference between the two metals, although the overall barriers are quite similar (27.9 vs 31.2 kcal mol^{-1}). Furthermore, the computations highlight that the concerted route can be considered as a general Lewis acid supported S–S cleavage mechanism, as the

availability of high oxidation states is, apparently, not crucial in stabilizing intermediate **D** and the direct transition structure for its formation ($\mathbf{TS_{AD}}$). Hence, this route might be responsible for the similarity of the experimental barriers across a wider range of cations.

The three competing mechanisms, a roaming radical route, an oxidative addition, and a Lewis acid supported mechanism are depicted in Scheme 2, where the distinction among routes a−c is a formal one to assist conceptual understanding. The balance among these pathways is subtle and depends on various factors such as the S−S bond strength, the availability of higher valence states, and the Lewis acidity of M^+. The computational results suggest the rearrangement of the title compound in the presence of Cu(I) to occur via oxidative addition; however, the gas-phase experiments do not provide conclusive evidence in this respect. Last, but not least, solvation effects supposedly exert a quite different influence on the oxidative addition and the Lewis-acid based pathways, which demands much more detailed investigations in the future.

CONCLUSIONS

Monitoring of the title reaction using electrospray ionization mass spectrometry reveals that the intramolecular redox reaction between the imine and disulfide moieties in the title compound **1** can proceed in the presence of a single copper ion.[2] In this work, we present a joined experimental and theoretical treatment of this process aimed to identify structures of the involved species, to characterize the role and oxidation state of the catalyst, and to provide a detailed mechanistic understanding of the title reaction. From the combined experimental and theoretical findings, the following main conclusions can be drawn:

(i) The observed parent ion formed during the electrospray ionization of the solution of the reactants corresponds to a four-coordinate complex of Cu(I) with the intact substrate.

(ii) Theory predicts the copper-catalyzed process to begin with S−S bond cleavage, either as a separate step, which is in fact an oxidative addition of copper into the S−S bond, or in a concerted manner with the formation of a C−S bond in a multicentered transition structure. Hydrogen atom transfer between the two parts of the substrate can then complete the redox reaction.

(iii) After the loss of the oxidized half of the substrate in the course of the copper-mediated disproportionation, the reduced part prefers coordination as a neutral imine thiophenol ligand in the major fragment ion.

(iv) Several cations other than copper can mediate the reaction in the gas phase. Exploratory computations suggest that the concerted pathway is feasible, if the metal shows sufficient Lewis acidity, whereas, in agreement with expectations, oxidative addition necessitates the availability of higher valence states. A roaming radical mechanism may be relevant in the case of less efficient catalysts and at elevated energies.

In the light of the present results, there seems to exist a pronounced competition of several mechanistic pathways. Computations suggest the copper(III)-catalyzed oxidative addition to have the lowest barrier in the gas phase; however, the lack of direct supporting experimental evidence and the expected large solvent effects on the different routes hamper translation of the derived mechanism to the preparative reaction in solution. While the gas-phase data provide helpful knowledge for the mechanistic understanding of the copper-mediated C−S coupling reaction, further studies addressing the effects of solvation are indicated to formulate a more complete picture of the reactions of copper species with disulfides.

ASSOCIATED CONTENT

Supporting Information. Energy profiles for alternative routes and the CuH elimination, breakdown graphs for CuH elimination, comparison of experimental IRMPD spectra with computations for several isomers, imaginary frequencies of transitional modes, M06 and spin-projected B3LYP results, $\langle S^2 \rangle$ values, CID spectra with additional cations, the full refs 56 and 57, Cartesian coordinates, and total energies of the computed structures. This material is available free of charge via the Internet at http://pubs.acs.org.

AUTHOR INFORMATION

Corresponding Author

*E-mail: lubos@uochb.cas.cz (L.R.), Detlef.Schroeder@uochb.cas.cz (D.S.).

Present Addresses

†LADIR, Univ. Pierre et Marie Curie, Paris, France.

ACKNOWLEDGMENT

This work was supported by the Czech Academy of Sciences (Z40550506), the Ministry of Education, Youth, and Sports of the Czech Republic (project LC512), and the European Research Council (AdG HORIZOMS). Further, we kindly appreciate the allocation of beam time at the IR laser center CLIO (IC 021-10), thank the entire team of CLIO for helpful assistance, and acknowledge travel support to CLIO within the ELISA scheme of the European Commission. Last, but not least, we greatly appreciate constructive criticisms of the reviewers that helped us to further improve the quality of the article and extend the scope of the study.

REFERENCES

(1) (a) Hartwig, J. F. *Nature* **2008**, *455*, 314. (b) Glueck, D. S. *Dalton Trans.* **2008**, 5276.

(2) Srogl, J.; Hyvl, J.; Révész, Á.; Schröder, D. *Chem. Commun.* **2009**, 3463.

(3) Hyvl, J.; Srogl, J. *Eur. J. Org. Chem.* **2010**, 2849.

(4) (a) Weekes, A. A.; Westwell, A. D. *Curr. Med. Chem.* **2009**, *16*, 2430. (b) Mortimer, C. G.; Wells, G.; Crochard, J.-P.; Stone, E. L.; Bradshaw, T. D.; Stevens, M. F. G.; Westwell, A. D. *J. Med. Chem.* **2006**, *49*, 179. (c) Chakraborty, M.; Jin, K. J.; Brewer, A. C.; Peng, H.-L.; Platz, M. S.; Novak, M. *Org. Lett.* **2009**, *11*, 4862. (d) Van Zandt, M. C.; Jones, M. L.; Gunn, D. E.; Geraci, L. S.; Jones, J. H.; Sawicki, D. R.; Sredy, J.; Jacot, J. L.; DiCioccio, A. T.; Petrova, T.; Mitschler, A.; Podjarny, A. D. J. Med. Chem. **2005**, *48*, 3141. (e) Rodrigues-Rodrigues, C.; de Groot, N. S.; Rimola, A.; Alvarez-Larena, A.; Lloveras, V.; Vidal-Gancedo, J.; Ventura, S.; Vendrell, J.; Sodupe, M.; Gonzalez-Duarte, P. *J. Am. Chem. Soc.* **2009**, *131*, 1436. (f) Huang, S.-T.; Hsei, I.-J.; Chen, C. *Bioorg. Med. Chem.* **2006**, *14*, 6106.

(5) (a) Yamashita, M.; Fenn, J. B. *J. Phys. Chem.* **1984**, *88*, 4451. (b) Fenn, J. B. *J. Am. Soc. Mass Spectrom.* **1993**, *4*, 524.

(6) Jayaweera, P.; Blades, A. T.; Ikonomou, M. G.; Kebarle, P. *J. Am. Chem. Soc.* **1990**, *112*, 2452.

(7) For the opposite, i.e., gas-phase evidence for a key role of binuclear clusters in Cu-mediated coupling reactions, see: (a) Roithová,

J.; Schröder, D. *Chem.—Eur. J.* **2008**, *14*, 2180. (b) Roithová, J.; Milko, P. *J. Am. Chem. Soc.* **2010**, *132*, 281.
(8) For recent reviews about the gas-phase chemistry of copper, see: (a) Tureček, F. *Mass Spectrom. Rev.* **2007**, *26*, 563. (b) Roithová, J.; Schröder, D. *Coord. Chem. Rev.* **2009**, *253*, 666.
(9) Antebi, S.; Alper, H. *Tetrahedron Lett.* **1985**, *26*, 2609.
(10) Hayter, R. G.; Humiec, F. S. *J. Inorg. Nucl. Chem.* **1964**, *26*, 807.
(11) Kondo, T.; Uenoyama, S.; Fujita, K.; Mitsudo, T. *J. Am. Chem. Soc.* **1999**, *121*, 482.
(12) Zanella, R.; Ros, R.; Graziani, M. *Inorg. Chem.* **1973**, *12*, 2736.
(13) Kuniyasu, H.; Ogawa, A.; Miyazaki, S.; Ryu, I.; Kambe, N.; Sonoda, N. *J. Am. Chem. Soc.* **1991**, *113*, 9796.
(14) (a) Que, L., Jr.; Tolman, W. B. *Angew. Chem., Int. Ed.* **2002**, *41*, 1114. (b) Cramer, C. J.; Tolman, W. B. *Acc. Chem. Res.* **2007**, *40*, 601.
(15) (a) Henze, W.; Gartner, T.; Gschwind, R. M. *J. Am. Chem. Soc.* **2007**, *129*, 11362. (b) Bartholomew, E. R.; Bertz, S. H.; Cope., S.; Murphy, M.; Ogle, C. A. *J. Am. Chem. Soc.* **2008**, *130*, 11244. (c) Gartner, T.; Henze, W.; Gschwind, R. M. *J. Am. Chem. Soc.* **2008**, *130*, 13718. (d) Poater, A.; Cavallo, L. *Inorg. Chem.* **2009**, *48*, 2340.
(16) Huffman, L. M.; Stahl, S. S. *J. Am. Chem. Soc.* **2008**, *130*, 9196.
(17) Brandt, P.; Södergren, M. J.; Andersson, P. G.; Norrby, P.-O. *J. Am. Chem. Soc.* **2000**, *122*, 8013.
(18) (a) King, A. E.; Huffman, L. M.; Casitas, A.; Costas, M.; Ribas, X.; Stahl, S. S. *J. Am. Chem. Soc.* **2010**, *132*, 12068. (b) Phipps, R. J.; Grimster, N. P.; Gaunt, M. J. *J. Am. Chem. Soc.* **2008**, *130*, 8172.
(19) Himo, F.; Lovell, T.; Hilgraf, R.; Rostovtsev, V. V.; Noodleman, L.; Sharpless, K. B.; Fokin, V. V. *J. Am. Chem. Soc.* **2005**, *127*, 210.
(20) Osako, T.; Ueno, Y.; Tachi, Y.; Itoh, S. *Inorg. Chem.* **2003**, *42*, 8087.
(21) (a) Houser, R. P.; Halfen, J. A.; Young, V. G., Jr.; Blackburn, N. J.; Tolman, W. B. *J. Am .Chem. Soc.* **1995**, *117*, 10745. (b) Itoh, S.; Nagagawa, M.; Fukuzumi, S. *J. Am. Chem. Soc.* **2001**, *123*, 4087. (c) Ueno, Y.; Tachi, Y.; Itoh, S. *J. Am. Chem. Soc.* **2002**, *124*, 12428.
(22) Hanss, J.; Krüger, H.-J. *Angew. Chem., Int. Ed.* **1996**, *35*, 2827.
(23) Desbenoît, N.; Galardon, E.; Frapart, Y.; Tomas, A.; Artaud, I. *Inorg. Chem.* **2010**, *49*, 8637.
(24) Osako, T.; Ueno, Y.; Tachi, Y.; Itoh, S. *Inorg. Chem.* **2004**, *43*, 6516.
(25) (a) Holthausen, M. C.; Fiedler, A.; Schwarz, H.; Koch, W. *Angew. Chem., Int. Ed. Engl.* **1995**, *34*, 2282. (b) Holthausen, M. C.; Koch, W. *Helv. Chim. Acta* **1996**, *79*, 1939. (c) Haynes, C. L.; Fisher, E. R.; Armentrout, P. B. *J. Phys. Chem.* **1996**, *100*, 18300. (d) Yi, S. S.; Blomberg, M. R. A.; Siegbahn, P. E. M.; Weisshaar, J. C. *J. Phys. Chem. A* **1998**, *102*, 395. (e) van Koppen, P. A. M.; Bowers, M. T.; Haynes, C. L.; Armentrout, P. B. *J. Am. Chem. Soc.* **1998**, *120*, 5704.
(26) (a) Matsumoto, K.; Sugiyama, H. *Acc. Chem. Res.* **2002**, *35*, 915. (b) Lobana, T. S.; Isobe, K.; Kitayama, H.; Nishioka, T.; Kinoshita, I. *Angew. Chem., Int. Ed.* **2004**, *43*, 213.
(27) (a) Schalley, C. A.; Wesendrup, R.; Schröder, D.; Weiske, T.; Schwarz, H. *J. Am. Chem. Soc.* **1995**, *117*, 7711. (b) Wesendrup, R.; Schalley, C. A.; Schröder, D.; Schwarz, H. *Chem.—Eur. J.* **1995**, *1*, 608. (c) Schalley, C. A.; Wesendrup, R.; Schröder, D.; Schroeter, K.; Schwarz, H. *J. Am. Chem. Soc.* **1995**, *117*, 12235. (d) Schalley, C. A.; Schröder, D.; Schwarz, H.; Möbus, K.; Boche, G. *Chem. Ber./Recueil* **1997**, *130*, 1085.
(28) Schalley, C. A.; Dieterle, M.; Schröder, D.; Schwarz, H.; Uggerud, E. *Int. J. Mass Spectrom. Ion Processes* **1997**, *163*, 101.
(29) Tintaru, A.; Roithová, J.; Schröder, D.; Charles, L.; Jušinski, I.; Glasovac, Z.; Eckert-Maksić, M. *J. Phys. Chem. A* **2008**, *112*, 12097.
(30) Cech, N. B.; Enke, C. G. *Mass Spectrom. Rev.* **2001**, *20*, 362.
(31) Schröder, D.; Weiske, T.; Schwarz, H. *Int. J. Mass Spectrom.* **2002**, *219*, 729.
(32) O'Hair, R. A. J. *Chem. Commun.* **2006**, 1469.
(33) (a) Tsierkezos, N. G.; Buchta, M.; Holý, P.; Schröder, D. *Rapid Commun. Mass Spectrom.* **2009**, *23*, 1550. (b) Agrawal, D.; Zins, E. L.; Schröder, D. *Chem. Asian J.* **2010**, *5*, 1667.
(34) (a) Révész, Á.; Milko, P.; Žabka, J.; Schröder, D.; Roithová, J. *J. Mass Spectrom.* **2010**, *45*, 1246. (b) Zins, E. L.; Pepe, C.; Schröder, D. *J. Mass Spectrom.* **2010**, *45*, 1253.
(35) MacAleese, L.; Simon, A.; McMahon, T. B.; Ortega, J. M.; Scuderi, D.; Lemaire, J.; Maitre, P. *Int. J. Mass Spectrom.* **2006**, *249*, 14.
(36) Chiavarino, B.; Crestoni, M. E.; Fornarini, S.; Lanucara, F.; Lemaire, J.; Maitre, P. *Angew. Chem., Int. Ed.* **2007**, *46*, 1995.
(37) Simon, A.; MacAleese, L.; Maitre, P.; Lemaire, J.; McMahon, T. B. *J. Am. Chem. Soc.* **2006**, *129*, 2829.
(38) Recent reviews: (a) Dopfer, O. *J. Phys. Org. Chem.* **2006**, *19*, 540. (b) Polfer, N. C.; Oomens, J. *Phys. Chem. Chem. Phys.* **2007**, *9*, 3804. (c) Asmis, K. R.; Sauer, J. *Mass Spectrom. Rev.* **2007**, *26*, 542. (d) MacAleese, L.; Maitre, P. *Mass Spectrom. Rev.* **2007**, *26*, 583.
(39) For the B3LYP functional, see: (a) Vosko, S. H.; Wilk, L.; Nusair, M. *Can. J. Phys.* **1980**, *58*, 1200. (b) Lee, C.; Yang, W.; Parr, R. G. *Phys. Rev. B* **1988**, *37*, 785. (c) Becke, A. D. *Phys. Rev. A* **1988**, *38*, 3098. (d) Becke, A. D. *J. Chem. Phys.* **1993**, *98*, 5648. (e) Stephens, P. J.; Devlin, F. J.; Chabalowski, C. F.; Frisch, M. J. *J. Phys. Chem.* **1994**, *98*, 11623.
(40) For the empirical description of dispersion, see: Grimme, S. *J. Comput. Chem.* **2006**, *27*, 1787.
(41) Noodleman, L. *J. Chem. Phys.* **1981**, *74*, 5737.
(42) Noodleman, L.; Peng, C. Y.; Case, D. A.; Mouesca, J.-M. *Coord. Chem. Rev.* **1995**, *144*, 199.
(43) Yamaguchi, K.; Takahara, Y.; Fueno, T.; Houk, K. N. *Theor. Chim. Acta* **1988**, *73*, 337.
(44) Kitagawa, Y.; Saito, T.; Ito, M.; Shoji, M.; Koizumi, K.; Yamanaka, S.; Kawakami, T.; Okumura, M.; Yamaguchi, K. *Chem. Phys. Lett.* **2007**, *442*, 445.
(45) Saito, T.; Nishihara, S.; Kataoka, Y.; Nakanishi, Y.; Matsui, T.; Kitagawa, Y.; Kawakami, T.; Okumura, M.; Yamaguchi, K. *Chem. Phys. Lett.* **2009**, *483*, 168.
(46) Kitagawa, Y.; Saito, T.; Nakanishi, Y.; Kataoka, Y.; Shoji, M.; Koizumi, K.; Kawakami, T.; Okumura, M.; Yamaguchi, K. *Int. J. Quantum Chem.* **2009**, *109*, 3641.
(47) Reiher, M. *Faraday Discuss.* **2007**, *135*, 97.
(48) Cremer, D. *Mol. Phys.* **2001**, *99*, 1899.
(49) Ruiz, E.; Cano, J.; Alvarez, S.; Alemany, P. *J. Comput. Chem.* **1999**, *20*, 1391.
(50) Wittbrodt, J. M.; Schlegel, H. B. *J. Chem. Phys.* **1996**, *105*, 6574.
(51) Weigend, F.; Ahlrichs, R. *Phys. Chem. Chem. Phys.* **2005**, *7*, 3297.
(52) Weigend, F. *Phys. Chem. Chem. Phys.* **2006**, *8*, 1057.
(53) Zhao, Y.; Truhlar, D. G. *Theor. Chem. Acc.* **2008**, *120*, 215.
(54) Merrick, J. P.; Moran, D.; Radom, L. *J. Phys. Chem. A* **2007**, *111*, 11683.
(55) (a) Milko, P.; Roithová, J.; Tsierkezos, N. T.; Schröder, D. *J. Am. Chem. Soc.* **2008**, *130*, 7186. (b) Milko, P.; Roithová, J. *Inorg. Chem.* **2009**, *48*, 11734.
(56) Ahlrichs, R. et al. *TURBOMOLE 6.2*, University of Karlsruhe, Forschungszentrum Karlsruhe GmbH, TURBOMOLE GmbH, 2010. See the Supporting Information for the complete reference.
(57) Frisch, M. J. et al. *Gaussian 09*, Revision A.02, Gaussian, Inc., Wallingford CT, 2009. See the Supporting Information for the complete reference.
(58) Flükiger, P.; Lüthi, H. P.; Portmann, S.; Weber, J. *Molekel 4.3*; Swiss National Supercomputing Centre CSCS: Manno, Switzerland, 2000.
(59) The C=N double bonds of **1** give rise to *E*−*Z* isomerism; the *E*,*E* isomer was used in the present calculations, which is preferred by 4.0 kcal mol^{-1} over the *E*,*Z* isomer in the case of **A**. The *E*−*Z* isomerization in this complex has a barrier of 22.7 kcal mol^{-1}.
(60) Neese, F. *J. Phys. Chem. Solids* **2004**, *65*, 781.
(61) For related works about the electronic structure of copper(III)-thiolate systems, see, for example: (a) Barone, G.; Silvestri, A.; Roos, B. O. *Phys. Chem. Chem. Phys.* **2005**, *7*, 2126. (b) Bruno, G.; Almeida, M.; Artizzu, F.; Dias, J. C.; Mercuri, M. L.; Pilia, L.; Rovira, C.; Ribas, X.; Serpec, A.; Deplano, P. *Dalton Trans.* **2010**, *39*, 4566.
(62) Concerning related features of the electronic structure of copper(III) organometallics, see: (a) Snyder, J. P. *J. Am. Chem. Soc.* **1995**, *117*, 11025. (b) Bera, J. K.; Samuelson, A. G.; Chandrasekhar, J. *Organometallics* **1998**, *17*, 4136.

(63) The M06 functional predicts $\mathbf{E_{NR}}$ to be somewhat more stable, falling between $\mathbf{E_N}$ and $\mathbf{E_S}$.

(64) Similarly to $\mathbf{E_{Cu}}$, the pertinent copper(III) hydride isomer $\mathbf{F_{Cu}}$ has very high energy ($\mathbf{F_{Cu}}$ + **2** is at 68.6 kcal mol^{-1} relative to **A**) and it was not taken into further consideration.

(65) Tyo, E. C.; Castleman, A. W., Jr.; Schröder, D.; Milko, P.; Roithová, J.; Ortega, J. M.; Cinellu, M. A.; Cocco, F.; Minghetti, G. *J. Am. Chem. Soc.* **2009**, *131*, 13009.

(66) The H/D exchange primarily occurs with solvent vapors in the source region, while association reactions strongly dominate in MS/MS experiments within the ion trap.

(67) Note that various rotamers are expected to have very similar IR spectra and these may accordingly contribute to the measured IRMPD patterns.

(68) (a) Schröder, D.; Schwarz, H.; Milko, P.; Roithová, J. *J. Phys. Chem. A* **2006**, *110*, 8346. (b) Schröder, D.; Ducháčková, L.; Jušinski, I.; Eckert-Maksić, M.; Heyda, J.; Tůma, L.; Jungwirth, P. *Chem. Phys. Lett.* **2010**, *490*, 14. (c) Schröder, D.; Ducháčková, L.; Tarábek, J.; Karwowska, M.; Fijalkowski, K.; Ončák, M.; Slavíček, P. *J. Am. Chem. Soc.* **2011**, *133*, 2444.

(69) (a) Moore, D. T.; Oomens, J.; Eyler, J. R.; von Helden, G.; Meijer, G.; Dunbar, R. C. *J. Am. Chem. Soc.* **2005**, *127*, 7243. (b) Polfer, N. C.; Oomens, J.; Dunbar, R. C. *Phys. Chem. Chem. Phys.* **2006**, *8*, 2744.

(70) For related IRMPD studies of microhydrated monocations, see: (a) Jagoda-Cwiklik, B.; Jungwirth, P.; Rulíšek, L.; Milko, P.; Roithová, J.; Lemaire, J.; Maitre, P.; Ortega, J. M.; Schröder, D. *ChemPhysChem* **2007**, *8*, 1629. (b) Jiang, L.; Wende, T.; Bergmann, R.; Meijer, G.; Asmis, K. R. *J. Am. Chem. Soc.* **2010**, *132*, 7398. (c) Sinha, R. K.; Nicol, E.; Steinmetz, V.; Maitre, P. *J. Am. Soc. Mass Spectrom.* **2010**, *21*, 758. (d) Paterová, J.; Heyda, J.; Jungwirth, P.; Shaffer, C. J.; Révész, Á.; Zins, E.-L.; Schröder, D. *J. Phys. Chem. A* **2011**, *115*, 6813. (e) Reference 68c.

(71) The kinetic shift in mass spectrometry arises from the fact that the time of observation in the experiment is limited such that species with energies only slightly above the threshold may not react to the products within the sampling time. See: Lifshitz, C. *Eur. J. Mass Spectrom.* **2002**, *8*, 85.

(72) (a) Armentrout, P. B. *Int. J. Mass Spectrom.* **2003**, *227*, 289. (b) Narancic, S.; Bach, A.; Chen, P. *J. Phys. Chem. A* **2007**, *111*, 7006. (c) Armentrout, P. B.; Ervin, K. M.; Rodgers, M. T. *J. Phys. Chem. A* **2008**, *112*, 10071.

(73) Kinetic shifts up to 1 eV (23 kcal mol^{-1}) were reported even for simple dissociations of transition-metal complexes much smaller than **1**/Cu$^+$. For an example, see: Meyer, F.; Khan, F. A.; Armentrout, P. B. *J. Am. Chem. Soc.* **1995**, *117*, 9740.